

Suzaku observation of the Phoenix Galaxy

G. Matt¹, S. Bianchi¹, H. Awaki², A. Comastri³, M. Guainazzi⁴, K. Iwasawa³, E. Jimenez-Bailon⁵, F. Nicastro⁶

¹Dipartimento di Fisica, Università degli Studi Roma Tre, via della Vasca Navale 84, I-00146 Roma, Italy

²Department of Physics, Faculty of Science, Ehime University, Bunkyo-cho, Matsuyama, Ehime 790-8577, Japan

³INAF - Osservatorio Astronomico di Bologna, via Ranzani 1, 40127 Bologna, Italy

⁴European Space Astronomy Center of ESA, Apartado 50727, 28080 Madrid, Spain

⁵Instituto de Astronomia, UNAM, Apartado 70264, 04510 Ciudad de Mexico, Mexico

⁶INAF - Osservatorio Astronomico di Roma, via Frascati 33, 00040 Monteporzio Catone, Roma, Italy

Received / Accepted

ABSTRACT

Context. In recent years, several Seyfert 2 galaxies have been discovered that change state when observed in X-rays a few years apart, switching from Compton-thin to reflection-dominated or viceversa.

Aims. We observed a member of this class of “Changing-look” sources, the Phoenix Galaxy, with *Suzaku*, with the aim of better understanding the nature of the variations.

Methods. The *Suzaku* spectrum was analyzed, and the results compared with previous ASCA and XMM-Newton observations.

Results. The source was caught in a Compton-thin state, as in XMM-Newton, but differently from ASCA. Comparing the *Suzaku* and XMM-Newton observations, a variation in the column density of the absorber on a time scale of years is discovered. A similar change, but on much shorter time scales (i.e. ks) may also explain the count-rate variations during the *Suzaku* observations. A soft excess is also present, likely due to continuum and line emission from photoionized circumnuclear matter.

Key words. Galaxies: active – X-rays: galaxies – Seyferts: individual: Phoenix Galaxy

1. Introduction

In recent years, it has been discovered that several Seyfert 2 galaxies change state when observed in X-rays a few years apart, switching back and forth from Compton-thin (i.e. absorbed by line-of-sight matter with column densities lower than $\sigma_T^{-1} = 1.5 \times 10^{24} \text{ cm}^{-2}$) to reflection-dominated (Guainazzi 2001; Guainazzi et al. 2002; Matt, Guainazzi & Maiolino 2003). There are at present 6 objects in this class, i.e. about 10% of the total population of reflection-dominated AGN in the local Universe (Guainazzi et al. 2005).

The Compton reflection dominated spectrum is usually assumed to be the result of Compton-thick absorption, the reflection being due to the far side of the obscuring torus (e.g. Matt 2002 and references therein). Therefore, the most obvious explanation for the change of state is the variation in the column density of the absorber. This is indeed the case in one changing-look source, NGC 1365 (Risaliti et al. 2005), where the column density is varying on very short time scale. However, in another case, NGC 2992, this behaviour is clearly due to huge flux variations in the nuclear radiation (Gilli et al. 2000): when the flux is very low, the reflection component (in this case clearly arising from rather distant matter) remains the only visible component, an echo of the source past activity. (This is what happened also in another famous source, NGC 4051, Guainazzi et al. 1998, which differs only because in the high flux state it is a Seyfert 1 instead of a Compton-thin Seyfert 2, and on a much lower flux scale also to our own Galactic centre, Koyama et al. 2008 and references therein). It is worth noting that in this scenario the Compton-thick reflecting matter and the Compton-thin absorber are likely

to be associated with different regions, the latter possibly being related to the host galaxy (e.g. Lamastra et al. 2006).

In the other sources of this class, the nature of the variations is still unclear, due to the lack of a proper monitoring campaign and/or of hard X-ray measurements. Here we report on the *Suzaku* observation of one of the brightest “Changing-look” source, the “Phoenix Galaxy”.

The Phoenix Galaxy (as christened by Guainazzi et al., 2002, now an NED recognised name; a.k.a. UGC 4203 and Mkn 1210) is a Seyfert 2 at $z=0.0135$. It was observed by XMM-Newton on May 2001 (Guainazzi et al. 2002), unveiling an X-ray bright nucleus (observed 2-10 keV flux of about $10^{-11} \text{ erg cm}^{-2} \text{ s}^{-1}$), absorbed by cold matter with $N_H \approx 2 \times 10^{23} \text{ cm}^{-2}$.

In an ASCA observation performed about five and half years earlier (Awaki et al. 2000, Guainazzi et al. 2002), the prominent iron line ($EW \approx 1 \text{ keV}$) and the factor-of-5 lower 2–10 keV flux indicated instead a reflection-dominated spectrum, with the nuclear emission too faint to be visible. The limited bandpass of ASCA could not permit checking whether the disappearing of the nucleus below 10 keV was due to an increase of the column density into a moderately Compton-thick regime. The lower limit to a putative absorber is about 10^{24} cm^{-2} .

2. Observation and data reduction

The Phoenix Galaxy was observed by *Suzaku* on 2007 May 2. X-ray Imaging Spectrometer (XIS) and Hard X-ray Detector (HXD) event files were reprocessed with the latest calibration files available (2008-07-09 release), using FTOOLS 6.5 and *Suzaku* software Version 9 and adopting standard filtering procedures. Source and background spectra for all the three XIS detectors were extracted from circular regions of 2.9 arcmin radius, avoid-

ing the calibration sources. Response matrices and ancillary response files were generated using `XISRMPGEN` and `XISSIMARFGEN`. We downloaded the “tuned” non-X-ray background (NXB) for our `HXD/PIN` data provided by the `HXD` team and extracted source and background spectra using the same good time intervals. The `PIN` spectrum was then corrected for dead time, and the exposure time of the background spectrum was increased by a factor 10, as required. Finally, the contribution from the cosmic X-ray background (CXB) was subtracted from the source spectrum, simulating it as suggested by the `HXD` team. The final net exposure times are 59 ksec for the three `XIS` spectra and 46 ksec for the `HXD/PIN` (the source was not detected with the `HXD/GSO`).

We also rereduced the *XMM-Newton* data again (OBSID 0002940701 - 5 May, 2001) with the latest calibration files. The observation was performed with the `EPIC` (European Photon Imaging Camera) CCD cameras, the p-n, and the two `MOS` (metal oxide semiconductors), operated in full window and thin filter. Data were reduced with `SAS 7.1.0`, and screening for intervals of flaring particle background was done consistently with the choice of extraction radii, in an iterative process based on the procedure to maximise the signal-to-noise ratio described by Piconcelli et al. (2004). The p-n was heavily affected by high background and resulted in a very short net exposure time (see G02) so will not be used in this paper. On the other hand, the net exposure time for the `MOS` cameras is 7634 s, adopting a source extraction radius of 14 arcsec and including patterns 0 to 12. The background spectra were extracted from source-free circular regions with a radius of 50 arcsec. Since the two `MOS` cameras were operated with the same mode, we co-added `MOS1` and `MOS2` spectra, after having verified that they agree with each other and with the summed spectrum.

3. Data analysis

3.1. Imaging and timing analyses

The only source present in the field of view of the `XIS` were the target itself. No bright sources are found in the *XMM-Newton* images, either. We extracted light curves from the `XIS` and `PIN` instruments. The 0.3-2 keV and 2-10 keV `XIS0+XIS1+XIS3` light curves are shown in Figs. 1 and 2. While the 0.3-2 keV light curves do not show any significant variation in the source emission, a clear increase in the flux is observed in the 2-10 keV light curve. This suggests that, above a few keV, the nucleus is directly visible, therefore that the source has been caught in a Compton-thin state.

No significant variability is observed in the `PIN`. The source is detected up to about 50 keV, with a 13-50 keV count rate of 0.074 ± 0.003 counts/s.

3.2. Spectral analysis. *Suzaku*

For the spectral analysis, we used the full complement of *Suzaku* instruments apart from the `XIS2`, no longer in use at the time of the observation, and the `GSO`, as the source is not detected with this instrument. We added a normalization constant for each instrument, fixing the value for `XIS0` to 1, and to 1.18 for the `PIN`, as appropriate for data taken at the `HXD` nominal position. The values for the `XIS1` and `XIS3` instruments were left free to vary, and turned out to be about 1.02 and 0.97, respectively. The energy bands are 0.5-10 keV for the `XIS` and 13-50 keV for the `HXD/PIN`.

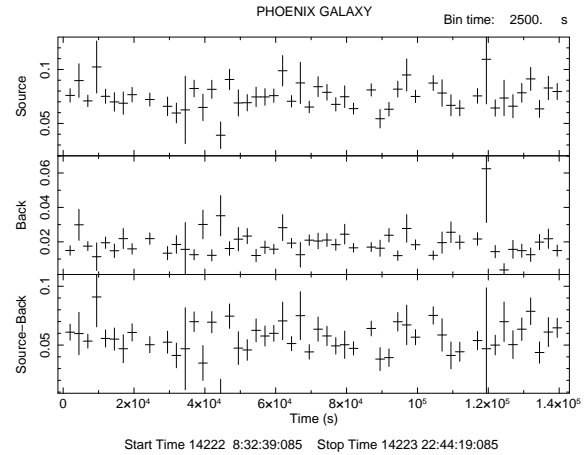


Fig. 1. The 0.3-2 keV total (upper panel), background (middle panel), and net source (lower panel) `XIS0+XIS1+XIS3` light curves for the *Suzaku* observations.

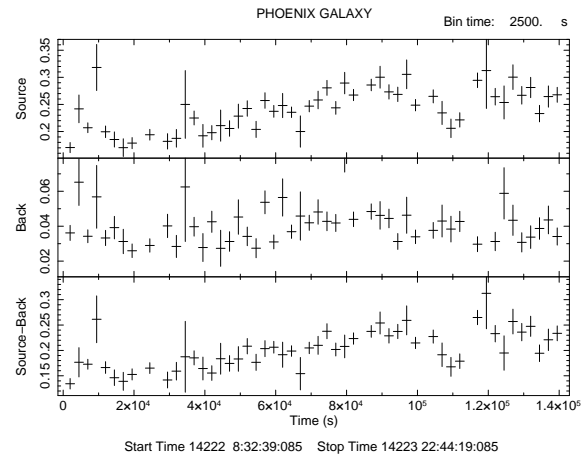


Fig. 2. The same as in the previous figure, but for the 2-10 keV band.

The fits were performed using the `XSPEC 12` software package. Errors refer to 90% confidence level for one interesting parameter.

3.2.1. The source status

Following previous results (G02), and with the aim of characterising the status of the source, we started fitting the data above 4 keV for simplicity in order to minimise the contribution from the soft X-ray component, whatever its origin (see below). We adopted a baseline model composed of: a power law; a Compton reflection (CR) component, with metal abundances fixed to the cosmic value (Anders & Grevesse 1989) and the inclination angle fixed to 30° ; a neutral and narrow iron line. All these components are seen through an absorber at the redshift of the source (absorption model `ZPHABS`¹; Thomson scattering is also considered including the model `CABS`). The fit is perfectly acceptable, $\chi^2_r/d.o.f.=0.92/150$. The best fit results are summarised in Table 1.

¹ Abundances set to the Anders & Grevesse 1989 values, cross sections from Balucinska-Church & McCammon (1992). See <http://heasarc.gsfc.nasa.gov/docs/xanadu/xspec/> for details.

An equally good fit ($\chi_r^2/d.o.f.=0.91/150$) is obtained if the reflection component is left outside the absorber. In this case the N_H is a bit larger ($4.19 \times 10^{23} \text{ cm}^{-2}$), the power law index is very similar (1.84), and the reflection component smaller (1.26).

As already suggested by the timing analysis, the source is Compton-thin, as in the XMM-*Newton* observation (Guainazzi et al. 2002) and differently from the ASCA observation, when it was Compton-thick. In fact, when fitting the *Suzaku* spectrum with a pure CR (Γ fixed to 2), the fit is much worse, $\chi_r^2/d.o.f.=1.80/152$; moreover, the iron line EW, about 240 eV, is far too low, see e.g. Ghisellini et al. (1994); Matt et al. (1996).

The 4-10 keV flux is $4.3 \times 10^{-12} \text{ erg cm}^{-2} \text{ s}^{-1}$ (XIS0), corresponding to a 2-10 keV unabsorbed flux of $1.9 \times 10^{-11} \text{ erg cm}^{-2} \text{ s}^{-1}$ and luminosity of $7.7 \times 10^{42} \text{ erg s}^{-1}$ ($H_0=70 \text{ km/s/Mpc}$). The index of the power law, Γ , and the relative normalization of the Compton reflection component, R , turned out to be highly correlated with each other; see Fig. 3. At the 2σ level, Γ can range from about 1.65 up to about 2.1, with R ranging correspondingly from about 1 up to 4. The value of the equivalent width of the iron line, about 200 eV, strongly favours the low Γ , low R scenario. In fact, for cosmic abundancies such a value of the iron line EW would correspond to a value of R in between 1 and 1.5 (e.g. Matt et al. 1991), not forgetting that part of the line (up to 50-60 eV for large covering factors, e.g. Matt et al. 2003) may originate in the absorber itself.

Adopting the model *ZWABS* instead of *ZPHABS* for absorption, rather different best-fit values are found, due to the different cross sections and abundancies adopted (Morrison & McCammon 1982; Anders & Ebihara 1982). The column density remains about the same ($3.26^{+0.28}_{-0.33} \times 10^{23} \text{ cm}^{-2}$) (as well as the quality of the fit: $\chi_r^2/d.o.f.=0.94/150$); but Γ is now $2.13^{+0.16}_{-0.17}$, while R becomes $5.2^{+4.8}_{-2.3}$, formally consistent within the errors with the values found using *ZPHABS*, but not allowing for the low R solution required by the iron line EW.

The presence of a Compton-thin absorber and a Compton-thick reflection indicates that more than one circumnuclear region does exist, as often observed in Seyfert 2s. To check this, we also fitted the data with a model developed by one of us (HA) and his collaborators (“Ehime” model, here-in-after: Ikeda et al. 2009). The model, based on MonteCarlo simulations, assumes that the absorption and reflection come from the same material, a torus with a half-opening angle which is one of the fitting parameters. The fit is still acceptable, $\chi_r^2/d.o.f.=1.13/150$, but significantly worse than that with the Compton-thick reflector. The best-fit column density is about $3.7 \times 10^{23} \text{ cm}^{-2}$, with a half opening angle of about 30° (but very poorly constrained to be within 10° and 50°) and $\Gamma \sim 1.5$. Allowing the absorbing and reflecting material to be different, not surprisingly, a fit as good as the one in Table 1 is recovered; the column density of the torus (now responsible only for the reflection) is $4.7 \times 10^{24} \text{ cm}^{-2}$, with a better determined half opening angle of 25^{+12}_{-4} degrees, and a slightly larger inclination angle.

3.2.2. Variability

As noted earlier, the source flux changes during the observation. In particular, it is consistently higher in the second half of the observation. To search for spectral variability, we divided the observation into two parts, the dividing time at about 50 ks (elapsed time) from the start of the observation. The resulting spectra (from now on denoted as “low” and “high”) have net exposures of 24 and 35 ks (XIS), and 4-10 keV count rates (XIS0) of 0.0445 ± 0.0015 and 0.0638 ± 0.0015 cts/s, respec-

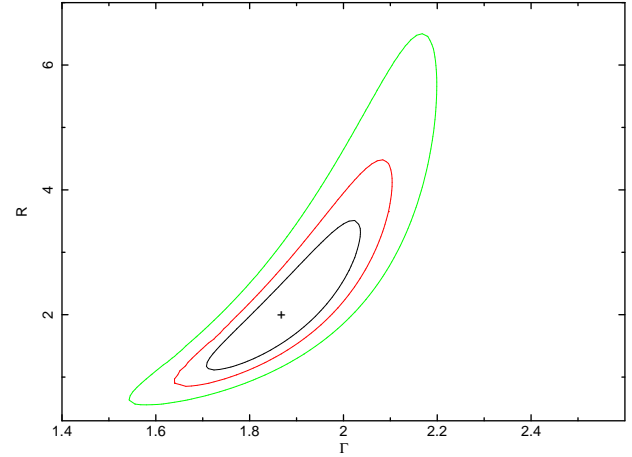


Fig. 3. The Γ - R contour plot, fitting the *Suzaku* spectrum above 4 keV.

tively (to be compared with a count rate in the total spectrum of 0.0577 ± 0.0011). The 13-50 keV count rates in the PIN are 0.070 ± 0.005 and 0.077 ± 0.004 .

The fits with the baseline model ($E > 4$ keV) are reported in Table 1. All spectral parameters are consistent with one another within the errors, indicating that the variation may be entirely due to a change in the normalization of the intrinsic flux. Indeed, forcing the two column densities to be the same and allowing the power law and the iron line normalizations, as well as the R , to vary, leads to an acceptable fit ($\chi^2/d.o.f.=1.14/69$). In the fit only XIS0 and PIN were used, to avoid complications in the fitting procedure due to the normalization constants between the three XISs. The small (or no) variability in the PIN is, in this fit, accounted for by the increase of R in the low state (best-fit values of 2.2 and 1.3, even if the two values are consistent each other within the very large errors), as expected if the reflecting matter is at large distances from the black hole.

On the other hand, the lack of significant variability in the PIN (the [13-50 keV]/[4-10 keV] hardness ratios in the two states are formally inconsistent with each other) may suggest that the change is entirely due to column density variations. Indeed, fitting simultaneously the “low” and “high” spectra letting only the N_H to vary, a better fit is found ($\chi^2/d.o.f.=1.11/71$). The contour plot between the two column densities is shown in Fig. 4, where it is seen that in this scenario the column density varies by about $0.6 \times 10^{23} \text{ cm}^{-2}$. Using all XIS detectors, a qualitatively similar result is found, but the error bars are significantly larger due to the above-mentioned cross-calibration uncertainties.

To summarise, the quality of the data is not good enough to firmly assess the nature of the observed count rate variability, even if the N_H variability seems to be slightly preferable, providing a better fit with only one parameter free to vary. In any case, because the spectral variability is low, if any, for the sake of simplicity we only consider the total spectrum in the following.

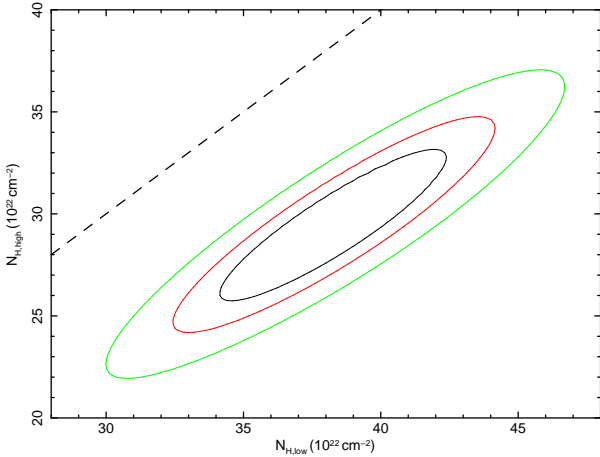
3.2.3. The iron line complex

The iron line energy of 6.398 ± 0.009 keV is perfectly consistent with neutral iron. If σ is left free to vary, no significant improvement in the quality of the fit is found; an upper limit of about 60 eV can be put to σ . Similarly, no improvement is found by adding a Compton Shoulder (CS; see e.g. Sunyaev & Churazov

Table 1. Best fit parameters for the baseline model, for $E > 4$ keV.

	Γ	N_H (10^{23} cm $^{-2}$)	R	E_{line} (keV)	F_{line} 10^{-5} ph cm $^{-2}$ s $^{-1}$	EW (eV)	χ_r^2 /d.o.f.	Flux (XIS0; 4-10 keV) 10^{-12} erg cm $^{-2}$ s $^{-1}$
Total	1.87 ± 0.18	$3.30^{+0.22}_{-0.23}$	$2.0^{+1.7}_{-0.9}$	6.398 ± 0.009	$4.34^{+0.55}_{-0.53}$	206 ± 26	0.91/150	4.26
Low	1.90 ± 0.33	$3.23^{+0.51}_{-0.66}$	$3.0^{+9.8}_{-2.1}$	$6.389^{+0.018}_{-0.024}$	$3.90^{+0.91}_{-0.86}$	228 ± 53	1.00/62	3.53
High	1.87 ± 0.22	$3.26^{+0.29}_{-0.28}$	$1.6^{+1.9}_{-0.9}$	$6.404^{+0.010}_{-0.015}$	$4.65^{+0.76}_{-0.72}$	200 ± 33	0.99/111	4.77

Note: from left to right: the index of the power-law (Γ); the column density of the intrinsic absorber; the relative normalization of the Compton reflection component, R ; the centroid energy, E_{line} , flux, F_{line} , and equivalent width (EW) of the iron line; the reduced χ^2 and the d.o.f.

**Fig. 4.** Contour plot for the column densities in the “low” and “high” states, assuming that the observed variability is entirely due to variations in the absorber (see text for details). The dashed line refers to the equal N_H relation.

1996; Matt 2002; Watanabe et al. 2003), assumed for simplicity to be a Gaussian with $\sigma=40$ eV centered at 6.32 eV (Matt 2002).

We also searched for the iron $K\beta$ (7.058 keV) and the nickel $K\alpha$ lines (7.472 keV). The upper limit to the fluxes are 5.0×10^{-6} (i.e. 12% of the iron $K\alpha$) and 5.8×10^{-6} (13% of the iron $K\alpha$), respectively. The upper limit to the $K\beta/K\alpha$ is consistent with low ionization (e.g. Molendi et al. 2003), in agreement with the line centroid energy. The upper limit to the nickel $K\alpha$ line is not particularly constraining, being consistent with an Ni/Fe ratio up to 3-4 times the cosmic value.

3.2.4. The soft excess

A significant emission in excess of the absorbed power law is clearly apparent in the spectrum (see Fig. 5). We first parametrized the soft excess with a power law (absorbed by the Galactic column, $N_{H,Gal}=3.45 \times 10^{20}$ cm $^{-2}$) with the index forced to be the same as that of the hard power law, as expected if the soft emission is due to Thomson reflection of the nuclear radiation. The fit is unacceptable (χ_r^2 /d.o.f.=1.71/231), with clear excesses below 2 keV. Allowing the two indices to vary independently, the fit slightly improves but remains unacceptable (χ_r^2 /d.o.f.=1.64/230). This is not surprising, as recent high resolution grating observations of Seyfert 2s have shown that most of the soft X-rays are due to emission lines (e.g. Guainazzi &

Table 2. Fluxes of the main emission lines expected in a photoionized plasma.

Line	Energy (keV)	Flux (10^{-6} ph cm $^{-2}$ s $^{-1}$)
O VII $K\alpha$	0.57	$29.1^{+23.5}_{-23.7}$
O VIII $K\alpha$	0.65	$16.3^{+10.6}_{-10.5}$
O VII RRC	0.74	$12.5^{+4.6}_{-4.6}$
O VIII RRC	0.87	$15.0^{+4.4}_{-3.0}$
Ne IX $K\alpha$	0.91	$4.9^{+3.0}_{-4.5}$
Fe xx L	0.965	$9.6^{+2.6}_{-7.1}$
Ne x $K\alpha$	1.02	< 7.0
Fe xxII L	1.053	$6.9^{+2.0}_{-4.6}$
Fe xxIII L	1.13	$3.7^{+2.3}_{-2.8}$
Fe xxIV L	1.17	< 3.3
Mg XI $K\alpha$	1.34	$1.5^{+1.2}_{-1.2}$
Si XIII $K\alpha$	1.85	< 2.1

Bianchi 2007, and references therein). Indeed, adding a thermal plasma component (MEKAL) dramatically improves the fit (χ_r^2 /d.o.f.=1.07/227). The temperature is $0.75^{+0.04}_{-0.07}$ keV, but the metal abundancies are unrealistically low ($0.09^{+0.01}_{-0.03}$) and the soft power law very flat ($\Gamma_s=0.12^{+0.14}_{-0.14}$). Indeed, the soft power law (of unknown origin) is required, because without it the fit is much worse (χ_r^2 /d.o.f.=1.61/229).

Alternatively, the lines may be emitted in photoionized, rather than collisionally ionized, plasma, as seems to be the case for most Seyfert 2s (Guainazzi & Bianchi 2007). We therefore substituted the MEKAL with many Gaussian, narrow-emission lines with the energy fixed to that of the most important transitions (see Table 2), even if there is no direct evidence from eye inspections of the spectrum for most of them. The two power law indices were forced to be the same (no significant improvement is found letting them vary independently). The fit is good (χ_r^2 /d.o.f.=1.16/219), even if not as good as the one with MEKAL. The presence of O VII and OVII radiative recombination continua (RRC) is in agreement with the assumption that the matter is indeed photoionized. The best fit values of N_H , Γ , R and the iron line EW for this fit are 3.33×10^{23} cm $^{-2}$, 1.71, 1.28 and 218 eV. The spectrum and best fit models are shown in Fig. 5 and Fig. 6, respectively, while the continuum parameters are summarized in

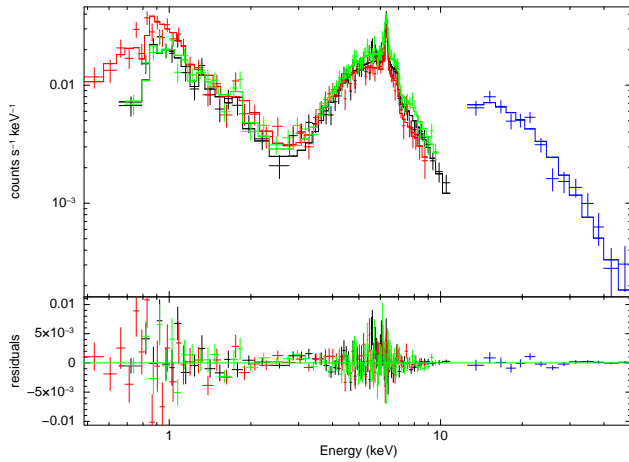


Fig. 5. Spectrum, best-fit model and residuals for the *Suzaku* observation. See text for details.

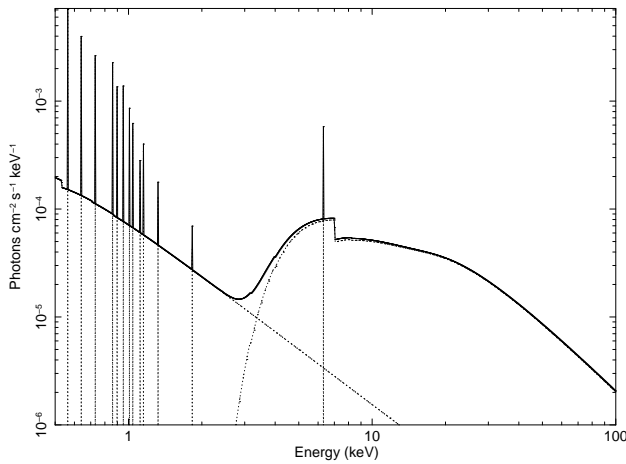


Fig. 6. The best-fit unfolded model. See text for details.

Table 3. From Fig. 6 it can be seen that the hard and soft components have similar fluxes at about 3 keV.

The observed 0.5-2 keV flux is 2.7×10^{-13} erg cm $^{-2}$ s $^{-1}$, 3.3% of the nuclear one, after correcting for absorption. This number is typical of Seyfert 2 galaxies (Bianchi & Guainazzi 2007). About 60% of the soft flux is in the continuum, and the remaining 40% in emission lines (adopting the photoionization scenario described above). Therefore, the column density of the photoionized matter, $N_{H,scatt}$, is $(0.6 \times 0.033) \sigma_T^{-1} (4\pi/\Delta\Omega)$, i.e. $3 \times 10^{22} (4\pi/\Delta\Omega)$ cm $^{-2}$, with $\Delta\Omega$ the solid angle subtended by the reflecting matter to the ionizing continuum. In a biconical geometry, $\Delta\Omega = 4\pi(1 - \cos\theta)$, with θ the half-opening angle. If $\theta = 25^\circ$, as suggested by the fit with the ‘‘Ehime’’ model, $N_{H,scatt} \sim 3 \times 10^{23}$ cm $^{-2}$.

3.3. Spectral analysis. XMM-Newton

The 0.5-10 keV XMM-Newton spectrum was fitted with a model similar to the one described in the previous paragraph, but letting the soft power-law index vary independently of the hard one. The reason is that the quality of the XMM-Newton spectrum is much lower than that of *Suzaku* due to the shorter exposure and the lack of p-n data, and the wealth of lines likely present in the soft band cannot be fitted individually. Only a line at about 0.9 keV, which is apparent in the data (see Guainazzi et al. 2002), is included. The best-fit values are summarised in Table 3.

The 4-10 keV flux is 9.5×10^{-12} erg cm $^{-2}$ s $^{-1}$, corresponding to a 2-10 keV unabsorbed flux of 2.6×10^{-11} erg cm $^{-2}$ s $^{-1}$ and luminosity of 1.1×10^{43} erg s $^{-1}$.

4. Comparison between *Suzaku* and XMM-Newton observations

After comparing the *Suzaku* and XMM-Newton observations, we first note that the intrinsic column density is higher (about 3.3×10^{23} against 1.8×10^{23} cm $^{-2}$). The difference is statistically significant (e.g., fixing the N_H in the XMM-Newton (*Suzaku*) observation to be equal to the *Suzaku* (XMM-Newton) best-fit value makes the fits much worse, $\Delta\chi^2 = 67$ (38)). This suggests that the absorber is relatively close to the nucleus, varying on timescales no longer than a few years.

The EW of the neutral iron line is about 200 eV in the *Suzaku* observation, more than in XMM-Newton data (but still consistent within the errors), while the line flux is about the same, i.e. 4.5×10^{-5} ph cm $^{-2}$ s $^{-1}$ against 3.9×10^{-5} ph cm $^{-2}$ s $^{-1}$; the two values are consistent each other within the errors. (The same is true if the line is put *outside* the absorber, in the hypothesis that the absorbing matter is closer to the black hole than the line emitting matter, in which case, the line fluxes are 1.9×10^{-5} and 2.4×10^{-5} ph cm $^{-2}$ s $^{-1}$.) The best-fit value of R is also higher, but consistent within the errors. (It is very poorly constrained in the XMM-Newton data due to the limited bandwidth.) The 2-10 keV XMM-Newton unabsorbed flux is about 1.5 times larger than the *Suzaku* one. As a result, we can conclude that the source was in a quite similar state during the *Suzaku* and XMM-Newton observations, albeit somewhat fainter in the former.

5. Discussion and conclusions

The main results from the 2007 *Suzaku* observation of the ‘‘changing-look’’ source, the Phoenix Galaxy (the first observation in hard X-rays, as the source was not observed by BeppoSAX), can be summarized as follows.

- The source was clearly in a Compton-thin state, as in 2001, when it was observed by XMM-Newton (Guainazzi et al. 2002), and differently than in 1995, when ASCA caught it in a reflection-dominated state (Awaki et al. 2000, Guainazzi et al. 2002).
- Guainazzi et al. (2002) interpreted the change of state from 1995 to 2001 in terms of a switching-on of the nuclear emission, which was off in the ASCA observation (having ‘‘re-birth’’ from its ashes, hence the ‘‘Phoenix’’ nickname). The (corrected for absorption) flux change from the XMM-Newton to the *Suzaku* observations (when it was about a factor 1.5 fainter) may support this scenario. On the other hand, the line-of-sight column density is different in the two observations, N_H being almost a factor 2 higher in the *Suzaku* data. The two values are inconsistent each other with high statistical significance, so the hypothesis that the change of state was due to variations in the absorber, as in NGC 1365 (Risaliti et al. 2005), cannot be ruled out, either.
- Variations in the column density of the absorber on hourly time scales may also explain the count rate variability observed during the *Suzaku* observation. (This interpretation is somewhat supported by the discovery of column density variations on weekly time scales in the *Chandra* data of this source: Risaliti et al., in preparation.) However, an explanation in terms of variations in the flux of the primary component cannot be excluded.

Table 3. Best fit parameters for the broad band *Suzaku* (photoionization scenario) and XMM-*Newton* spectra.

	Γ_s	Γ_h	N_H (10^{23} cm^{-2})	R	E_{line} (keV)	EW (eV)	$\chi_r^2/\text{d.o.f.}$
<i>Suzaku</i>	1.71±0.12	(= Γ_s)	3.33 $^{+0.17}_{-0.15}$	1.28 $^{+0.81}_{-0.56}$	6.397±0.009	218±24	1.16/219
XMM- <i>Newton</i>	2.49±0.23	1.62 $^{+0.11}_{-0.23}$	1.76 $^{+0.13}_{-0.21}$	<2.1	6.44±0.05	133±63	1.21/70

Note: from left to right: the indices of the soft (Γ_s) and hard (Γ_h) power laws; the column density of the intrinsic absorber; the relative normalization of the Compton reflection component, R ; the centroid energy, E_{line} and equivalent width (EW) of the iron line; the reduced χ^2 and the d.o.f.

- There is a significant reflection component, which implies a large amount of circumnuclear Compton–thick matter (e.g. Matt et al. 2003) even when the source is Compton–thin. The fit is not able to tell us if the reflecting matter is within or outside the absorber. Because the latter is varying on yearly time scales, and possibly on much shorter ones, it could not be too far away from the nucleus. Therefore, if the reflector is within the absorber, the natural candidate would be the accretion disc, the “torus” if it is outside. Within the admittedly large (especially for the short XMM-*Newton* observation) errors, the amount of the reflection component and of the iron line are constant between 2001 and 2007, suggesting emission from distant matter.
- The soft X-ray emission is fitted well by both a photoionised and a collisionally ionized material. However, the former solution is to be preferred, because it is more self-consistent (the collisionally plasma model requires the presence of a (very flat) power law, too, and very low abundancies) and because of the detection of the O VII and VIII radiative recombination continua.

Matt G., 2002, RSPTA, 360, 204
 Matt G., Guainazzi M., Maiolino R., 2003, MNRAS, 342, 422
 Molendi S., Bianchi S., Matt G., 2003, MNRAS, 343, L1
 Piconcelli E., Jimenez-Bailon E., Guainazzi M., et al., 2004, MNRAS, 351, 161
 Sunyaev R.A., Churazov E.M., 1996, Astr. Letters, 22, 648
 Watanabe S., Sako M., Ishida M., et al., 2003, ApJ, 597, L37

Acknowledgements

GM and SB acknowledge financial support from ASI under grants I/023/05/0 and I/088/06/0.

References

- Anders E., Ebihara M., 1982, Geo. Cosm. Acta, 46, 2363
 Anders E., Grevesse N., 1989, Geo. Cosm. Acta, 53, 197
 Arnaud K. A., 1996, in Jacoby G. H., Barnes J., eds, ASP Conf. Ser. Vol. 101, Astronomical Data Analysis Software and Systems V. Astron. Soc. Pac., San Francisco, p. 17
 Awaki H., Ueno S., Taniguchi Y., Weaver K.A., 2000, ApJ, 542, 175
 Baluinska-Church M., McCammon D., 1992, ApJ, 400, 699
 Bianchi S., Guainazzi M., 2007, AIP Conference Proceedings, Volume 924, pp. 822
 Gilli R., Maiolino R., Marconi A., et al., 2000, A&A, 355, 485
 Ghisellini G., Haardt F., Matt G., 1994, MNRAS, 267, 743.
 Guainazzi M., Nicastro F., Fiore F., et al., 1998, MNRAS, 301, L1
 Guainazzi M., 2001, MNRAS, 329, L13
 Guainazzi M., Matt G., Fiore F., Perola G.C., 2002, A&A, 388, 787
 Guainazzi M., Fabian A.C., Iwasawa K., Matt G., Fiore F., 2005a, MNRAS, 356, 295
 Guainazzi M., Matt G., Perola G.C., 2005, A&A, 444, 119
 Guainazzi M., Bianchi S., 2007, MNRAS, 374, 1290
 Ikeda S., Awaki H., Terashima Y., 2009, ApJ, in press
 Koyama K., Inui T., Matsumoto H., Tsuru T.G., 2008, PASJ, 60, 201
 Lamastra A., Perola G.C., Matt G., 2006, A&A, 449, 551
 Matt G., Perola G. C., Piro L., 1991, A&A, 247, 25
 Matt G., Brandt W.N., Fabian A.C., 1996, MNRAS, 280, 823
 Matt G., 2002, MNRAS, 337, 147